

Bound states in the continuum induced via local symmetries in complex structures

Cheng-Zhen Wang,¹ Ulrich Kuhl,² Adin Dowling,¹ Holger Schanz,³ and Tsampikos Kottos^{1,*}

¹*Wave Transport in Complex Systems Lab, Department of Physics,
Wesleyan University, Middletown, CT-06459, USA*

²*Université Côte d'Azur, CNRS, Institut de Physique de Nice (INPHYNI), 06200, Nice, France*

³*University of Applied Sciences Magdeburg–Stendal, 39114 Magdeburg, Germany*

Bound states in the continuum (BICs) defy conventional wisdom that assumes a spectral separation between propagating waves, that carry energy away, and spatially localized waves corresponding to discrete frequencies. They can be described as resonance states with infinite lifetime, i.e., leaky modes with zero leakage. The advent of metamaterials and nanophotonics allowed the creation of BICs in a variety of systems. Mainly, BICs have been realized by destructive interference between outgoing resonant modes or exploiting engineered global symmetries that enforce the decoupling of a symmetry-incompatible bound mode from the surrounding radiation modes. Here, we introduce theoretically BICs relying on a different mechanism, namely *local* symmetries that enforce a field concentration on a part of a complex system without implying any global symmetry. We experimentally implement such BICs using microwaves in a *compact* one-dimensional photonic network and show that they emerge from the annihilation of two topological singularities, a zero and a pole, of the measured scattering matrix. Our alternative for achieving BICs in complex wave systems may be useful for applications like sensing, lasing, and enhancement of nonlinear interactions that require high- Q modes.

INTRODUCTION

Quantum mechanics books, typically, distinguish between two type of states: bound states whose discrete energy lies below the continuum threshold (identified by the asymptotic value of the potential at infinity) and unbounded scattering states with an energy inside the continuum. Examples where these two categories of states appear include electrons in the presence of finite potential wells, quantum dots, or atomic potentials. An exception to the quantum *communis intellectus* are bound states in the continuum (BICs) [1–4]. These are spatially bounded solutions of the Schrödinger equation, with discrete eigenvalues lying inside the continuum of states that propagate to infinity. They were originally introduced a century ago by von Neumann and Wigner, using an inverse potential engineering approach [5]. The method assumed a square-integrable BIC wavefunction with a spatially decaying envelope and, using this as a starting point, they tailored a suitable 3D potential where this wavefunction is an eigenmode. Such “custom-made” potentials are unrealistic as they are oscillatory in space while decaying to infinity as a power law and they have never been implemented experimentally.

BICs are not a quantum phenomenon but rather pertain to all wave systems. This observation extended the search for BICs to a variety of other platforms including electromagnetic, acoustic, water or elastic waves (for a review see [1, 4]). Among the various areas, optics and photonics have undoubtedly been the tip of the spear as far as novel realizations of BICs are concerned [1–3, 6–11]. For example, an inverse design scheme based on supersymmetric transformations has been implemented in coupled optical waveguide arrays to engineer the hopping rate between nearest resonators in order to support

BICs [12].

Other, more efficient, BIC schemes have been also developed and experimentally implemented thanks to the advent of metamaterials and nanotechnology [1–3]. Perhaps the most prominent approach that also highlights the wave nature of the phenomenon, is associated with “accidental” BICs [13, 14]. In this case, the parameters of the target system are fine-tuned to achieve cancellation of outgoing waves to the continuum. A special case of accidental BIC is associated with Fabry-Perot (FP) configurations [8, 15, 16] of two identical resonances which interact strongly through the same radiation channel (e.g. a waveguide). A third mechanism that leads to BICs is invoking structures with geometric symmetries [1, 4, 17]. In this case, a trapped mode with a given symmetry can be embedded into a continuum of states with a distinct symmetry, ensuring the decoupling of the trapped mode and thus the suppression of its leakage.

Most of the above BIC proposals have been realized in extended structures. In fact, there is a non-existence theorem for BICs in compact structures [1] (see, however, Refs [18, 19] for exceptions). Finding a genuine BIC in compact systems is a challenging fundamental problem, and its solution would allow the implementation of high- Q resonators having a broad range of potential applications including lasers, sensors, filters and low-loss fibers [1, 4].

Here we provide an alternative approach for the implementation of BICs which is based on *local* symmetries (see Fig. 1a). As opposed to the symmetry-protected BICs, we study structures lacking geometric symmetries. The proposed mechanism relies on the existence of an embedded symmetric subdomain and reveals another backdoor in the non-existence theorem for BICs in compact structures. In contrast to accidental BICs [1, 4], our con-

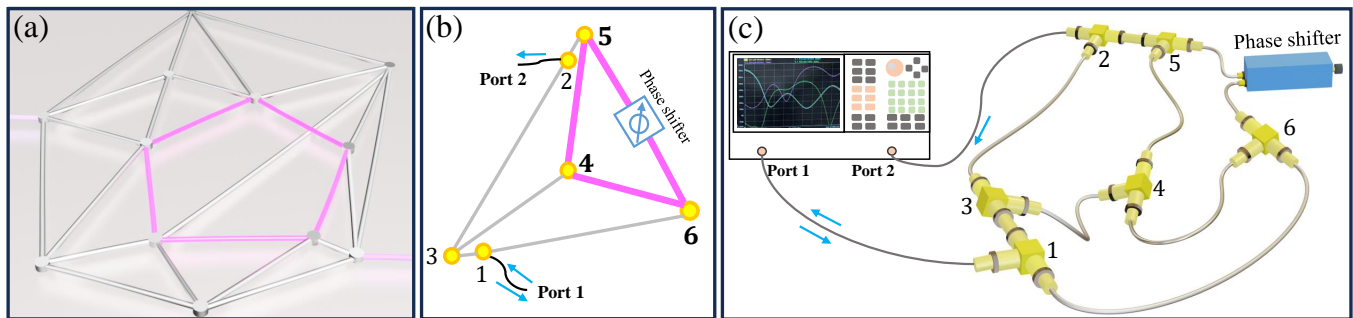


FIG. 1. **Experimental setup of a microwave graph detecting bound states in the continuum (BICs) based on local symmetries.** (a) Schematic representation of a complex network supporting a BIC due to the presence of a subnetwork (cycle) with a local symmetry (red-shaded equilateral pentagon). (b) Schematic representation of the network used in our experiment. A "tetrahedron" contains an equilateral triangle where one side length can be varied. The network is opened by two attached scattering channels. (c) The microwave tetrahedron network used in our experiments. Coaxial cables are connected by T-junctions at each of the vertices $n = 1, 2, \dots, 6$. Between vertices 5 and 6, we replace the cable with a phase shifter allowing us to vary the effective length between these vertices. The reflection amplitudes r_{11} , r_{22} and the transmission amplitudes t_{12} , t_{21} are measured using a vector network analyzer (VNA) connected to the vertices 1 and 2, respectively.

struction relies on a stringent blueprint and allows to analytically predict and control the position of BICs in the spectrum. Moreover, it leads to an infinite ladder of BIC states which occur periodically in k -space. We experimentally demonstrate the new scheme using a complex network of coaxial microwave cables coupled together via T-junctions, see Figs. 1b,c. The analysis of the experimental scattering matrix demonstrates that the formation of these BICs originates from the coalescence of two topological defects with opposite charges: a zero (with charge +1) and a pole (with charge -1) of the scattering matrix. Experimental implementations of such networks have been reported in a variety of frameworks including acoustics [20], microwaves [21–26], photonic crystal waveguides [27] and optics [28, 29].

PHYSICAL MECHANISM FOR LOCAL-SYMMETRY PROTECTION OF BICS

Let us explain the *local-symmetry* protection mechanism using complex photonic networks as an example (Fig. 1a): the subdomain (subnet) that possesses a local symmetry is formed by a closed loop (ring) of N_l equilateral edges such that mirror symmetry (with respect to the vertices defining the subnet) and discrete rotation invariance is guaranteed (see, for example, the violet pentagon in Fig. 1a with $N_l = 5$ or the violet triangle in Fig. 1b with $N_l = 3$ having a discrete rotational symmetry C_{5v} , C_{3v} , respectively). Note that in the case of a network that is formed by photonic waveguides, the geometric shape of the edges and the angles between them are typically irrelevant, see Fig. 1c. In this case the discrete rotation must not be interpreted in physical space. For example, in case of Fig. 1b, an angle is defined as $2\pi x/3\ell$ where x is a continuous path length along the cy-

cle and $x = 0$ coincides with a vertex. Then the subnet that supports a BIC is invariant under the transformations $x \rightarrow x + \ell$ and $x \rightarrow -x$, generating the symmetry group C_{3v} .

Consider the ring first without any connections to the remaining network. Then, choosing the appropriate symmetry class, there are rotation invariant eigenfunctions which are antisymmetric with respect to the vertices. That is, we have eigenfunctions vanishing at all vertices of the subnet. Thus, when the remaining network is coupled to some or all vertices of the subnet via coupling constants (not necessarily equal at all vertices), these eigenstates remain unaltered. In particular, if the remaining network is open and has a continuous spectrum, the constructed eigenfunctions will be BICs. This conclusion applies only to the subset of eigenstates pertaining to the appropriate symmetry class. All other states of the subnet will be strongly mixed with the states of the remaining network and in the large network limit the overwhelming majority of states will be ergodically distributed over the whole network, as expected for typical systems with wave chaos [30].

Note that the term *local* symmetry does not imply a subnet with a small total bond-length; rather it refers to the fact that it involves a subset of connected edges. In particular, the BIC might be supported by a subnet that connects distant parts of the total network either by involving a few long edges or many short ones.

While pure BICs are completely decoupled and do not contribute to transport across the network, any small perturbation of the subnet will create quasi-BICs which act as channels across the network and thus strongly affect its transport properties. The above BIC-mechanism is independent of specific properties of the network like the precise boundary conditions at the vertices or their valency (= the number of connected edges). Most im-

portantly it does not require any geometric symmetry of the network as a whole.

TRANSPORT IN COMPLEX NETWORKS AND BIC FORMATION

Scattering on Complex Networks — We study the scattering on a complex network of $n = 1, \dots, N$ vertices, where two vertices n, m may be connected by an edge $E = (n, m)$ with length l_E . The position $x_E = x$ on edge E is $x = 0(l_E)$ on vertex $n(m)$. The wave $\psi_E(x)$ on the edge E satisfies the Helmholtz equation

$$\frac{d^2}{dx^2}\psi_E(x) + k^2\psi_E(x) = 0, \quad (1)$$

where $k = \omega n_r / c_0$ is the wave number, ω is the angular frequency, c_0 is the speed of light, and n_r is the complex-valued relative index of refraction that includes the losses of the coaxial cables. The solution of Eq. (1) is $\psi_E(x) = \phi_n \frac{\sin k(l_E - x)}{\sin kl_E} + \phi_m \frac{\sin kx}{\sin kl_E}$, where $\psi_E(0) = \phi_n$ and $\psi_E(l_E) = \phi_m$ are the values of the field at the vertices. We turn the compact network to a scattering set-up by attaching transmission lines (TLs) $\alpha = 1, \dots, L$ to a subset of the vertices. The field on the α th TL takes the form $\psi_\alpha(x) = \mathcal{I}_\alpha e^{-ikx} + \mathcal{O}_\alpha e^{+ikx}$ for $x \geq 0$ where $x = 0$ is the position of the vertex. The coefficients \mathcal{I}_α (\mathcal{O}_α) indicate the amplitude of the incoming (outgoing) wave on the TLs. At each vertex n , continuity of the wave and current conservation are satisfied. These conditions can be expressed in a compact form as [31]

$$(M + iW^T W)\Phi = 2iW^T \mathcal{I}, \quad (2)$$

where $\Phi = (\phi_1, \phi_2, \dots, \phi_N)^T$. The L dimensional vector \mathcal{I} contains the amplitudes \mathcal{I}_α of the incident field, while W is a $L \times N$ matrix describing the connection between the TLs and the vertices. A matrix element $W_{\alpha,n}$ is 1, if the α th TL is attached to vertex n and zero otherwise. The $N \times N$ matrix M

$$M_{nm} = \begin{cases} -\sum_{l \neq n} \mathcal{A}_{nl} \cot kl_{nl}, & \text{if } n = m \\ \mathcal{A}_{nm} \csc kl_{nm}, & \text{if } n \neq m \end{cases} \quad (3)$$

incorporates information about the metric (length of edges) and the connectivity of the network, where \mathcal{A} is the adjacency matrix having elements $\mathcal{A}_{nm} = 1$ whenever two vertices m, n are connected and $\mathcal{A}_{nm} = 0$ otherwise.

The scattering field Φ on the compact part of the graph can be evaluated by solving Eq. (2) for Φ . The same expression, together with the continuity condition at the vertices, where the TLs are attached, can be used for deriving the scattering matrix [31]

$$S(k) = -\hat{I} + 2iW \frac{1}{M(k) + iW^T W} W^T. \quad (4)$$

For wavenumbers which are integer multiples of π/l_{nl} the terms M_{nm} diverge; this can be rectified by appropriate manipulation of the divergent terms, see [32].

The poles of the scattering matrix in the complex k -plane are related to resonances i.e. purely outgoing solutions of the wave equation and they are found from the condition $\det(M(k_p) + iW^T W) = 0$. Of interest are also the zeroes of the scattering matrix defined via the secular equation $\det S(k_z) = 0$. For lossless structures, causality implies $k_z = k_p^*$. The zeroes $S(k) = 0$ correspond to a special type of wavefronts with time-modulated amplitude, known as coherent virtual absorption, which are temporarily trapped inside the structure without any leakage [33, 34]. When Ohmic losses are also included, one can find parameters of the structure for which the complex zeroes cross the real axis. In this case, there are stationary, perfectly impedance-matched input wavefronts which are completely absorbed by the (weakly) lossy elements in the structure which acts as an interferometric trap, known as coherent perfect absorber [35]. The exceptional case where the poles are equal to the zeroes of the S -matrix corresponds to BIC states which contain neither an incoming nor an outgoing radiation component and exist at a real frequency of passive structures. Thus a BIC is invariant under time reversal and it does not affect the on-shell scattering matrix $S(k)$ since it is decoupled from the far-field radiation. In the topological-defect picture in the complex k -plane a BIC implies that a charge +1 (S -matrix zero) annihilates with a charge -1 (resonance) on the real axis. We have confirmed experimentally this topological feature (see below).

BIC and quasi BIC states — We now identify the conditions that are required for the realization of locally symmetric BIC states on a complex network. To this end, we consider a subgraph consisting of C edges that form a closed loop within the network (for example, in Fig. 1a, $C = 5$ for the violet pentagon). We assume that they have equal lengths ℓ and construct a state $\psi_c(x) = \sqrt{(2/C\ell)} \sin(k_M x)$ which is restricted to this cycle. This requires $k_M = M\pi/\ell$ and $k_M = 2M\pi/\ell$ ($M = 1, 2, \dots$) for even and odd C , respectively. The above wave function is zero at the vertices along the subgraph. Therefore the state is not affected by further edges attached to these vertices which couple the subgraph to the surrounding network and to the continuum. This argument is completely independent of the topology of the rest of the network, the number of extra edges that are attached to the vertices of the cycle, and the number of attached TLs. Further considerations reveal that it is possible to relax the assumption of equal edge lengths ℓ on the subgraph to rationally related lengths. Importantly, the above construction is just a special case of the symmetry argument given in the introduction which may apply also in different situations.

In an experiment, the BICs are manifested as long-lived quasi-bound (resonant) states that disappear and reappear in a characteristic manner when the edge lengths along the subgraph are changed by a small

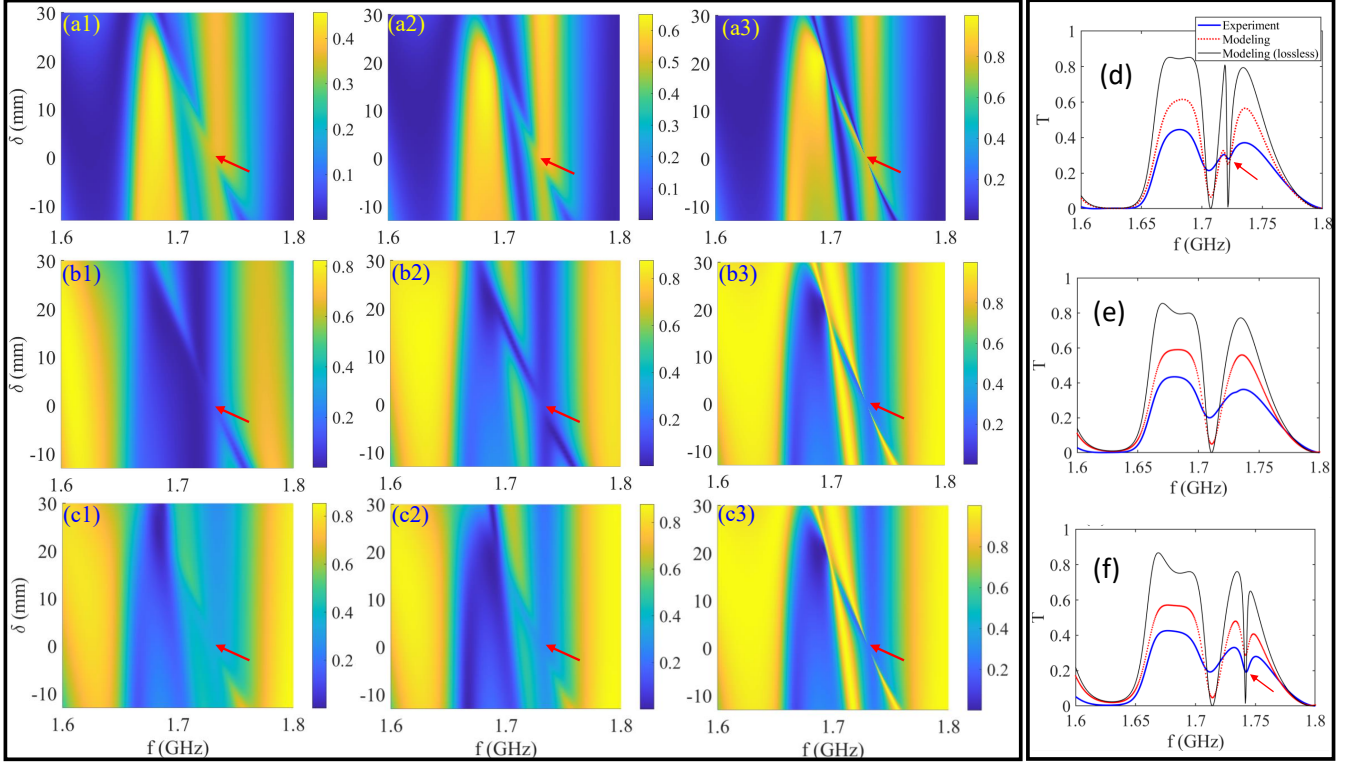


FIG. 2. **The transmittance and reflectance spectrum versus the phase shifter length variation δ and frequency f .** (a1) The experimental measurements of the transmittance through the graph (input from lead 1, transmittance is the same as that from lead 2 due to reciprocity) versus the input frequency and phase-shifter length variation δ . (a2) and (a3) the same as in (a1) but for the theoretical modeling with adjusted loss and without loss, respectively. (b1)-(b3) The reflectance from lead 1 versus the input frequency and phase-shifter variation δ for experimental measurement, theoretical modeling with loss, and theoretical modeling without loss, respectively. (c1)-(c3) The same plot as in (b1)-(b3) for reflectance from lead 2. (d)-(f) The cross-section plot of transmittance T for $\delta = 6, 0$, and -6 mm respectively. The blue solid, red dotted and black solid lines are for the experimental measurement, theoretical modeling with fitted loss and theoretical modeling without loss, respectively.

amount δ . The values of the wave field at the connections to the remaining network and the TLs are now $\psi_c(0) \sim k\delta$. Due to this coupling, a BIC gives rise to a Feshbach resonance with width $\gamma \sim |\delta|^2$. The latter reveals itself as a sharp feature in the transmittance $T(f)$ and left (right) reflectance $R_1(f)$ ($R_2(f)$), where $R_1 = R_2$ if there are no losses inside the network. This feature is absent when $\delta = 0$ and this is an indirect, but experimentally observable, signature of a BIC in scattering data.

EXPERIMENTAL IMPLEMENTATION

We consider the tetrahedron network shown in Figs. 1b,c. This network is relatively simple and it does not have any geometrical symmetries. At the same time, the dynamics is rich enough to show typical features of wave chaos [30, 31, 36, 37]. Its microwave implementation is done using coaxial cables (Huber+Suhner S 04272) connected by 6 T-junctions (vertices). The electrical permittivity of the cables was found to be

$\epsilon \approx 1.56(\pm 0.07) + i0.0015(\pm 0.0005)$ indicating the presence of uniform losses. Two TLs have been attached at the vertices labeled 1 and 2, see Figs. 1b,c.

We choose the triangle consisting of the vertices 4, 5, and 6 as the closed loop that supports BICs. The electrical lengths $l_{45} = l_{46} = \ell = 346.6$ mm are fixed while the length l_{56} of the third edge varies such that $l_{56} = \ell + \delta$ with $\delta \in [-14, 30]$ mm (see Supplementary Material). The length-variation is done using a phase shifter whose effective length is controlled electronically. Following the theoretical arguments of the previous section we expect that BICs will appear at $\delta = 0$, for wavenumbers $k_M = 2M\pi/\ell$, $M \in \mathbb{N}^+$ corresponding to frequencies $f_M = M \frac{c_0}{\ell} = M \times 0.86547$ GHz. The other lengths of the network are $l_{13} = l_{25} = 18.2$ mm, $l_{23} = 424.2$ mm, $l_{16} = 926.5$ mm, and $l_{34} = 831.4$ mm.

In Figs. 2a1, b1, and c1, we report the measured transmittance T and reflectances R_1 and R_2 versus the input frequency and the tuning parameter δ in the proximity of the 2nd BIC frequency (2×0.86547 GHz ≈ 1.73 GHz) indicated by the arrow. The second (third) column reports

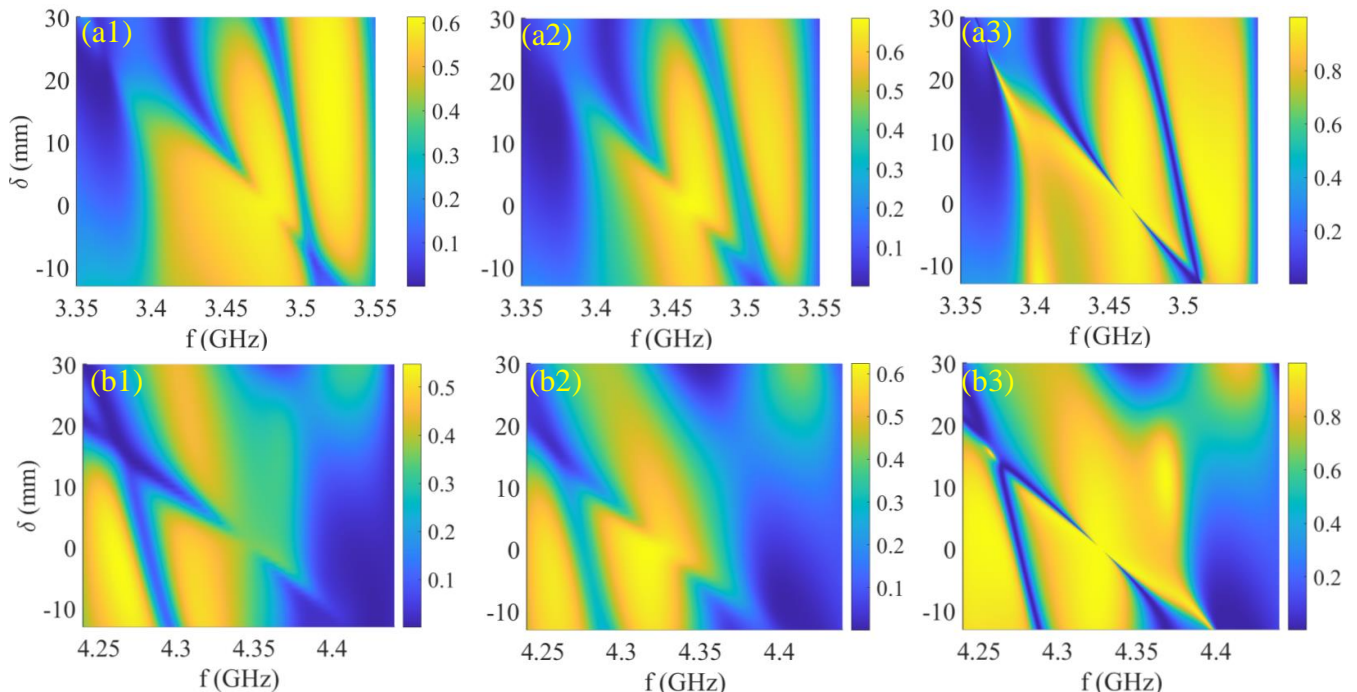


FIG. 3. **Transmittance spectra at frequencies that are multiples of the fundamental BIC frequency.** (a1)-(a3) The transmittance as a function of input frequency and bond variation δ for the experimental measurement (a1), the theoretical modeling with loss (a2) and without loss (a3) for the 4th BIC state at $4 \times 0.86547 \text{ GHz} \approx 3.46 \text{ GHz}$. (b1)-(b3) The same as in (a1)-(a3) but for the 5th BIC state at 4.33 GHz .

our calculations for the network of Fig. 1b,c in the presence (absence) of Ohmic losses at the coaxial cables. In the frequency range $f \in [1.6, 1.8] \text{ GHz}$, a BIC is predicted at $f_2 \approx 1.73 \text{ GHz}$. In all cases we find a resonance moving linearly from around 1.7 GHz at $\delta = 15 \text{ mm}$ to 1.76 GHz at $\delta = -10 \text{ mm}$. At $\delta = 0 \text{ mm}$ a BIC is formed and the resonance feature disappears from all three spectra ($T(f)$ and $R_{1,2}(f)$). This is the expected indirect signature of the BIC: since the state is completely decoupled from the rest of the network and the TLs, any incident radiation cannot excite it and therefore there are no signatures of its existence in the scattering matrix elements. Instead, for small $\delta \neq 0$, the transmittance $T(f \sim f_M)$ and reflectance $R(f \sim f_M)$ show a narrow resonance structure in their frequency-dependence whose width is controlled by the parameter δ . All these features of the transmittance and reflectance spectra are present in our measurements and in both sets of calculations (with and without losses). The presence of losses, however, smooths out some of the sharp characteristics of the (quasi-)BIC resonance (first and second columns) which are much more pronounced in the calculations shown in the third column where we have considered the same network without any losses of the coaxial cables.

To further investigate the variations of the resonance features in $T(f)$ as the tuning parameter changes around $\delta = 0$ we plot in the right column of Fig. 2, the trans-

mittance spectrum for three different δ values around the BIC value. For $\delta = 6 \text{ mm}$ (Fig. 2d) a narrow resonance dip (indicated by the red arrow) is evident in both, measurements (blue solid line) and calculations (red dotted line), where the Ohmic losses of the cables are taken into account. This dip becomes very sharp in the case of a lossless network modeling (black solid line). When $\delta = 0 \text{ mm}$, (Fig. 2e), the resonance dip disappears in all cases and reappears again when $\delta = -6 \text{ mm}$, (Fig. 2f), after acquiring a small blue-shift.

We have also confirmed experimentally the appearance of a cascade of bound states at predetermined k -values which are multiples of a “fundamental” BIC frequency and distinguish our approach from accidental BICs. To demonstrate this feature, we report in Fig. 3 the transmittance versus frequency and δ in different frequency regions where we expect the BIC to occur, i.e., $f = 3.35 - 3.55 \text{ GHz}$, and $f = 4.24 - 4.44 \text{ GHz}$. The same behavior as the one found for the BIC presented in Fig. 2 is observed here as well. Namely, we observe the appearance and disappearance of a quasi-BIC mode as δ varies, signifying the formation of BICs at $\delta = 0$.

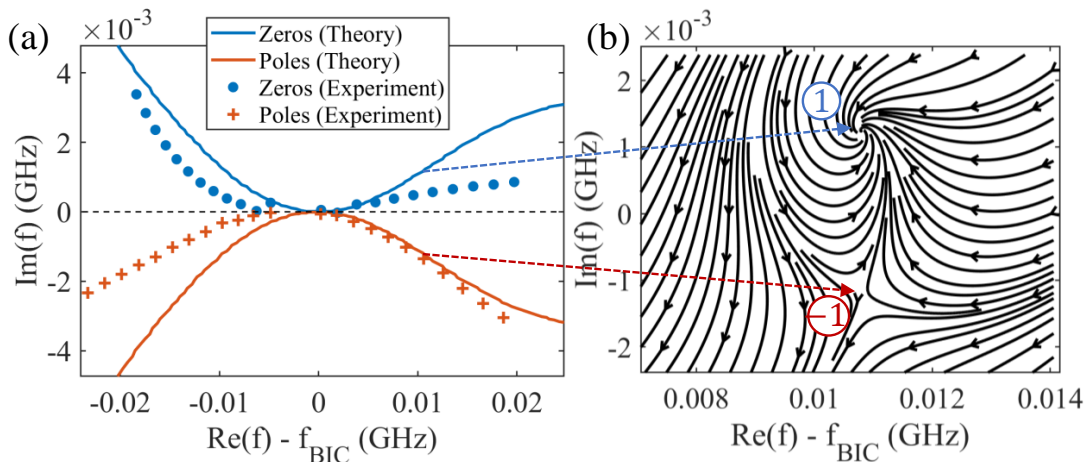


FIG. 4. **Formation of a BIC with local symmetry via the annihilation of a zero and a pole pair.** (a) Parametric evolution of poles (red) and zeros (blue) of the scattering matrix over the cable length l_{56} of the tetrahedron network of Fig. 1b,c for $\delta \in [-12, 12]$ mm. The experimental poles (red crosses) and zeros (blue-filled circles) have been extracted from the measured S -matrix. The numerical results are indicated with lines of the respective color and have been extracted from the S -matrix given by Eq. 4. All data have been shifted along the $\text{Im}(k)$ axis by 0.00314 due to the global loss induced by the Ohmic resistances in the coaxial cables. The $f_{\text{scar}} = 1.7309$ GHz corresponding to the BIC in Fig. 2. (b) Streamlines of the vector field $\vec{\Psi} = -\nabla_{\vec{k}} \arg(\det(S(\vec{k})))$ with $\vec{k} = (\text{Re}(k), \text{Im}(k))$, showing +1 and -1 topological charges at zeros and poles of the S -matrix corresponding to a $\delta = -6$ mm.

POLES, ZEROS, AND THE TOPOLOGICAL STRUCTURE OF BICS

Finally, we analyze the formation of BICs from a topological perspective [38] by analyzing the parametric evolution of the poles and zeros in the complex frequency plane as δ is changing. In Fig. 4a the symbols represent the poles (red crosses) and zeros (blue-filled circles) of the S -matrix that have been extracted from the measured S -matrix using the harmonic inversion method [39]. The method was applied to the off-diagonal elements of the S -matrix for the poles and to the matrix S^{-1} for the zeroes. Our data indicate their coalescence at $\delta = 0$ and at the BIC-frequency f_{BIC} as discussed above. The solid lines correspond to the simulations. The formation of the BIC in the complex $\vec{k} = (\text{Re}(k); \text{Im}(k))$ plane, is a consequence of the annihilation of two topological defects of the secular function $\det S(\vec{k})$ [38]: a zero \vec{k}_z and a pole \vec{k}_p of the scattering matrix which collides as the perturbation parameter δ vanishes (see Fig. 4a). The zero (pole) is characterized by the topological charge $q \equiv \frac{1}{2\pi} \oint d\vec{k} \cdot \nabla_{\vec{k}} \phi(\vec{k}) = +1$ ($q = -1$) which describes how many times the total phase of the scattering matrix $\phi(k) = \arg(\det S(k))$ winds by 2π along a counterclockwise simple closed path that encloses the topological defect (see Fig. 4b). A non-zero charge $q \neq 0$ indicates that a zero or a pole cannot suddenly disappear when the parameter δ slightly varies, although they can move in the complex \vec{k} -plane. Only a collision of a +1 charge with a -1 charge can result in their mutual annihilation, which signifies that at this parameter value δ a resonance mode

and a zero mode coexist.

CONCLUSION

We have revealed a physical mechanism based on local symmetries that leads to the creation of BICs in compact photonic networks without any geometrical symmetry. The resulting BICs are formed as a consequence of the collision of two topological defects (a pole and zero of the scattering matrix) which leads to their annihilation. The proposed BICs differ from scenarios, where BICs are formed due to the presence of a global symmetry or where they are the "accidental" result of a parameter variation. In particular, they do not require the degeneracy of two (or more) resonant modes and they are based on a precise rule that allows to construct and control a ladder of BIC states at multiples of a fundamental frequency. Our microwave demonstration can be extended to other wave platforms ranging from optics to acoustics and water waves and provides a new way of achieving and utilizing BICs in complex systems.

* tkottos@wesleyan.edu

- [1] C. W. Hsu, B. Zhen, A. D. Stone, J. D. Joannopoulos, and M. Soljacic, "Bound states in the continuum," *Nature Reviews Materials* **1**, 1 (2016).
- [2] Shereena Joseph, Saurabh Pandey, Swagato Sarkar, and Joby Joseph, "Bound states in the continuum in resonant nanostructures: an overview of engineered materials

- for tailored applications,” *Nanophotonics* **10**, 4175–4207 (2021).
- [3] Shaimaa I. Azzam and Alexander V. Kildishev, “Photonic bound states in the continuum: From basics to applications,” *Advanced Optical Materials* **9**, 2001469 (2021).
 - [4] Almas F Sadreev, “Interference traps waves in an open system: bound states in the continuum,” *Reports on Progress in Physics* **84**, 055901 (2021).
 - [5] J. von Neumann and E. P. Wigner, “Über merkwürdige diskrete eigenwerte,” in *The Collected Works of Eugene Paul Wigner: Part A: The Scientific Papers*, edited by Arthur S. Wightman (Springer Berlin Heidelberg, Berlin, Heidelberg, 1993) pp. 291–293.
 - [6] Bo Zhen, Chia Wei Hsu, Ling Lu, A. Douglas Stone, and Marin Soljačić, “Topological nature of optical bound states in the continuum,” *Phys. Rev. Lett.* **113**, 257401 (2014).
 - [7] Yu Guo, Meng Xiao, and Shanhui Fan, “Topologically protected complete polarization conversion,” *Phys. Rev. Lett.* **119**, 167401 (2017).
 - [8] D. C. Marinica, A. G. Borisov, and S. V. Shabanov, “Bound states in the continuum in photonics,” *Phys. Rev. Lett.* **100**, 183902 (2008).
 - [9] Yonatan Plotnik, Or Peleg, Felix Dreisow, Matthias Heinrich, Stefan Nolte, Alexander Szameit, and Mordechai Segev, “Experimental observation of optical bound states in the continuum,” *Phys. Rev. Lett.* **107**, 183901 (2011).
 - [10] Jiajun Wang, Lei Shi, and Jian Zi, “Spin hall effect of light via momentum-space topological vortices around bound states in the continuum,” *Phys. Rev. Lett.* **129**, 236101 (2022).
 - [11] Hugo M. Doeleman, Francesco Monticone, Wouter den Hollander, Andrea Alù, and A. Femius Koenderink, “Experimental observation of a polarization vortex at an optical bound state in the continuum,” *Nature Photonics* **12**, 397 (2018).
 - [12] G. Corrielli, G. Della Valle, A. Crespi, R. Osellame, and S. Longhi, “Observation of surface states with algebraic localization,” *Phys. Rev. Lett.* **111**, 220403 (2013).
 - [13] H. Friedrich and D. Wintgen, “Physical realization of bound states in the continuum,” *Phys. Rev. A* **31**, 3964–3966 (1985).
 - [14] H. Friedrich and D. Wintgen, “Interfering resonances and bound states in the continuum,” *Phys. Rev. A* **32**, 3231–3242 (1985).
 - [15] Chia Wei Hsu, Bo Zhen, Song-Liang Chua, Steven G Johnson, John D Joannopoulos, and Marin Soljačić, “Bloch surface eigenstates within the radiation continuum,” *Light: Science & Applications* **2**, e84 (2013).
 - [16] Steffen Weimann, Yi Xu, Robert Keil, Andrey E. Miroshnichenko, Andreas Tünnermann, Stefan Nolte, Andrey A. Sukhorukov, Alexander Szameit, and Yuri S. Kivshar, “Compact surface fano states embedded in the continuum of waveguide arrays,” *Phys. Rev. Lett.* **111**, 240403 (2013).
 - [17] M. Robnik, “A simple separable hamiltonian having bound states in the continuum,” *Journal of Physics A: Mathematical and General* **19**, 3845 (1986).
 - [18] Michał Lawniczak, Jiří Lipovský, Małgorzata Białous, and Leszek Sirko, “Application of topological resonances in experimental investigation of a fermi golden rule in microwave networks,” *Physical Review E* **103**, 032208 (2021).
 - [19] Ilya Deriy, Ivan Toftul, Mihail Petrov, and Andrey Bogdanov, “Bound states in the continuum in compact acoustic resonators,” *Phys. Rev. Lett.* **128**, 084301 (2022).
 - [20] M Röntgen, O Richoux, G Theocharis, C V Morfonios, P Schmelcher, P del Hougne, and V Achilleos, “Equireflectionality and customized unbalanced coherent perfect absorption in asymmetric waveguide networks,” (2023), arXiv:2305.02786v1.
 - [21] O. Hul, S. Bauch, P. Pakoński, N. Savvitsky, K. Życzkowski, and L. Sirko, “Experimental simulation of quantum graphs by microwave networks,” *Phys. Rev. E* **69**, 056205 (2004).
 - [22] A. Rehemangiang, M. Allgaier, C. H. Joyner, S. Müller, M. Sieber, U. Kuhl, and H.-J. Stöckmann, “Microwave realization of the gaussian symplectic ensemble,” *Phys. Rev. Lett.* **117**, 064101 (2016).
 - [23] Lei Chen and Steven M. Anlage, “Use of transmission and reflection complex time delays to reveal scattering matrix poles and zeros: Example of the ring graph,” *Phys. Rev. E* **105**, 054210 (2022).
 - [24] Junjie Lu, Jiongning Che, Xiaodong Zhang, and Barbara Dietz, “Experimental and numerical investigation of parametric spectral properties of quantum graphs with unitary or symplectic symmetry,” *Phys. Rev. E* **102**, 022309 (2020).
 - [25] Markus Allgaier, Stefan Gehler, Sonja Barkhofen, H.-J. Stöckmann, and Ulrich Kuhl, “Spectral properties of microwave graphs with local absorption,” *Phys. Rev. E* **89**, 022925 (2014).
 - [26] L. Chen, T. Kottos, and S.M. Anlage, “Perfect absorption in complex scattering systems with or without hidden symmetries,” *Nature Communications* **11**, 5826 (2020).
 - [27] Shukai Ma, Thomas M. Antonsen, and Steven M. Anlage, “Eigenfunction and eigenmode-spacing statistics in chaotic photonic crystal graphs,” *Phys. Rev. E* **106**, 054215 (2022).
 - [28] Hadiseh Nasari, Georgios G. Pyrialakos, Demetrios N. Christodoulides, and Mercedeh Khajavikhan, “Non-hermitian topological photonics,” *Opt. Mater. Express* **13**, 870–885 (2023).
 - [29] Stefano Lepri, Cosimo Trono, and Giovanni Giacomelli, “Complex active optical networks as a new laser concept,” *Phys. Rev. Lett.* **118**, 123901 (2017).
 - [30] F. Haake, S. Gnutzmann, and M. Kuś, *Quantum Signatures of Chaos* (Springer Series in Synergetics, 2019).
 - [31] Tsampikos Kottos and Uzy Smilansky, “Chaotic scattering on graphs,” *Phys. Rev. Lett.* **85**, 968 (2000).
 - [32] Tsampikos Kottos and Uzy Smilansky, “Periodic orbit theory and spectral statistics for quantum graphs,” *Annals of Physics* **274**, 76–124 (1999).
 - [33] Denis G. Baranov, Alex Krasnok, and Andrea Alù, “Coherent virtual absorption based on complex zero excitation for ideal light capturing,” *Optica* **4**, 1457–1461 (2017).
 - [34] S. Longhi, “Coherent virtual absorption for discretized light,” *Opt. Lett.* **43**, 2122–2125 (2018).
 - [35] Y. D. Chong, Li Ge, Hui Cao, and A. D. Stone, “Coherent perfect absorbers: Time-reversed lasers,” *Phys. Rev. Lett.* **105**, 053901 (2010).

- [36] Tsampikos Kottos and Uzy Smilansky, “Periodic orbit theory and spectral statistics for quantum graphs,” *Ann. Phys.* **274**, 76–124 (1999).
- [37] H. Schanz and T. Kottos, “Scars on quantum networks ignore the lyapunov exponent,” *Phys. Rev. Lett.* **90**, 234101 (2003).
- [38] William R. Sweeney, Chia Wei Hsu, and A. Douglas Stone, “Theory of reflectionless scattering modes,” *Phys. Rev. A* **102**, 063511 (2020).
- [39] U. Kuhl, R. Höhmann, J. Main, and H.-J. Stöckmann, “Resonance widths in open microwave cavities studied by harmonic inversion,” *Phys. Rev. Lett.* **100**, 254101.

Supplemental Material

for manuscript: “Bound states in the continuum induced via local symmetries in complex structures”

Cheng-Zhen Wang¹, Ulrich Kuhl², Adin Dowling¹, Holger Schanz³, and Tsampikos Kottos¹

¹ Wave Transport in Complex Systems Lab, Department of Physics, Wesleyan University, Middletown, CT-06459, USA

² Université Côte d’Azur, CNRS, Institut de Physique de Nice (INPHYNI), 06200 Nice, France

³ University of Applied Sciences Magdeburg–Stendal, 39114 Magdeburg, Germany

Experimental Characterization of the Complex Network

To determine the parameters entering the numerical simulation, we have measured the different cable lengths as $l_{16} = 726$ mm, $l_{34} = 644$ mm, $l_{23} = 310$ mm, and $l_{45} = l_{46} = 245.7$ mm. Have in mind that the real length is also including lengths from the T junctions which are 18 mm. Additionally we assume that the phase-shifters optical length is equivalent to the optical length of cable l_{45} when we have $\delta = 0$ mm corresponding to a fixed real length of the phase shifter. We extract the complex refractive index n of the cables and phase-shifter based on the transmission measurements. Comparing the wave propagation through the coaxial cable, to the Helmholtz equation for a 1D free and uniform medium, we can get the transmission coefficient t as

$$t = \frac{\psi(l)}{A} = e^{i\frac{\omega}{c}\text{Re}(n)l} e^{-\frac{\omega}{c}\text{Im}(n)l}, \quad (\text{S.1})$$

where we have the refractive index as $n = \sqrt{\epsilon_0}$, $\omega = 2\pi f$ the angular frequency, and the cable length l . First, we can get the real part of t as

$$\text{Re}(t) = \cos\left[\frac{\omega}{c}\text{Re}(n)l\right] e^{-\frac{\omega}{c}\text{Im}(n)l}, \quad (\text{S.2})$$

where we can see the cos terms is oscillation part, which could give us the $\text{Re}(n)$ based on our measured t in a frequency range and measured cable length l . Second, the imaginary part of refractive index n can be obtained based on the transmittance $T = |t|^2$ which is of the form of

$$T = |t|^2 = e^{-\frac{2\omega}{c}\text{Im}(n)l}, \quad (\text{S.3})$$

where we can get $\text{Im}(n)$ by fitting the curve of transmittance versus frequency for certain cable length l . To avoid the influence of the SMA connector effect on the

cable length, in our measurement, we use the ratio of transmission t_1/t_2 for two cables with different length l_1, l_2 . In this way, we only need the cable length difference so that we can get rid of the error from the SMA connector and get more accurate $\text{Re}(n)$ and $\text{Im}(n)$. By fitting the transmission curves, we get $\text{Re}(n) = 1.212$ and $\text{Im}(n) = 0.002$ for coaxial cables. For the phase shifter, we obtain the refractive index as $\text{Re}(n) = 1.004$ and $\text{Im}(n) = 0.002$. Note, that the $\text{Im}(n)$ is frequency dependent, which we ignored thus taking only an average n for the whole investigated frequency range into account.

The electrical length of the cables and phase shifter are defined as the measured geometrical length multiply the real part of refractive index. We have the δ to characterize the phase shifter geometrical length shift with $\delta = 0$ corresponding to a total electrical length of phase shifter equals to be that of l_{46} and increase δ corresponding increasing the electrical length of phase shifter.

In our modeling, to get better fit for the theory with experiment, we adopt the measured cable lengths and the complex refractive index, as well as the T junction length as the central value, and give each variable a fluctuation range. Then, we use surrogate optimization method in Matlab to find the parameter set that gives the best fit for the transmittance and reflectance curves over the whole 0.5 – 6.5 GHz range. The fitted geometrical lengths are $l_{16} = 764.4$ mm, $l_{34} = 686$ mm, $l_{23} = 350$ mm, $l_{45} = l_{46} = 286$ mm, $l_{13} = l_{25} = 15$ mm, refractive index for cable is $n_c = 1.212 + 0.0022i$, and refractive index for phase shifter is $n_p = 1.004 + 0.002i$. The slight difference with respect to the geometrically measured physical lengths of the cables is attributed to the presence of T-junctions that add an additional length that has to be included in the modeling and the precision that the permittivities of the cables have been extracted. For the phase shifter the electrical length is $\tilde{l}_{56} = 286 \cdot n_c + \delta \cdot n_p$, with δ the detuning parameter and the imaginary part of the length representing loss.